Nonlinear Reconstruction

Hong-Ming Zhu,[1, 2] Yu Yu,[3] Ue-Li Pen,[4, 5, 6, 7] Xuelei Chen,[1, 2, 8] and Hao-Ran Yu[9, 4]

[1]*Key Laboratory for Computational Astrophysics, National Astronomical Observatories,*
Chinese Academy of Sciences, 20A Datun Road, Beijing 100012, China
[2]*University of Chinese Academy of Sciences, Beijing 100049, China*
[3]*Key Laboratory for Research in Galaxies and Cosmology, Shanghai Astronomical Observatory,*
Chinese Academy of Sciences, 80 Nandan Road, Shanghai 200030, China
[4]*Canadian Institute for Theoretical Astrophysics, University of Toronto,*
60 St. George Street, Toronto, Ontario M5S 3H8, Canada
[5]*Dunlap Institute for Astronomy and Astrophysics, University of Toronto,*
50 St. George Street, Toronto, Ontario M5S 3H4, Canada
[6]*Canadian Institute for Advanced Research, CIFAR Program in*
Gravitation and Cosmology, Toronto, Ontario M5G 1Z8, Canada
[7]*Perimeter Institute for Theoretical Physics, 31 Caroline Street North, Waterloo, Ontario, N2L 2Y5, Canada*
[8]*Center of High Energy Physics, Peking University, Beijing 100871, China*
[9]*Kavli Institute for Astronomy and Astrophysics, Peking University, Beijing 100871, China*
(Dated: November 23, 2016)

We present a direct approach to non-parametrically reconstruct the linear density field from an observed non-linear map. We solve for the unique Displacement potential consistent with the non-linear density and positive definite Coordinate transformation using a multi grid algorithm. We show that we Recover the linear initial conditions up to $k \sim 1$ with minimal computational cost.

This reconstruction approach generalizes the linear displacement theory to fully non-linear Fields, potentially substantially expanding the BAO and RSD information content of dense Large scale structure surveys, including for example SDSS main sample and 21cm intensity mapping.

Introduction.—The observation of large scale structure of the Universe is a cornerstone of modern cosmology. Several ambitious surveys are mapping large swaths of the visible universe (e.g. CHIME, DESI, PFS, etc). Precision measurements of the power spectrum and two-point correlation function are continually improving. However, the precision of the measurement of baryon acoustic oscillations, redshift space distortions, primordial non-Gaussianity, etc, from the two-point statistics is often limited by strong non-Gaussianity of the dark matter and galaxy density fields on small scales, which prevent a simple mapping to the initial conditions that are predicted by cosmological theories. The loss of coherence to the initial conditions has been known as mode-mode coupling, information saturation, etc. Some of the couplings are understood as arising from the coupling of large scale linear modes to smaller scale still linear modes (e.g. Tides [1, 2], Supersample covariance [3]). These can be corrected by a linear mapping, also known as "reconstruction" [4](cite Seo, Padmanabhan, etc).

Recent work showed that the $z = 0$ Lagrangian space non-linear displacement potential correlates with the initial linear field (arxiv 1610.07112) to a $k \sim 2h/$Mpc, about an order of magnitude shorter length scale than observed in Eulerian space. That worked required knowing the actual displacement of dark matter particles, which in practice is not observable. In this paper we implement the combination of the mass ordering coordinate of 1609.07041 with the E-mode displacement field, resulting in a unique solution that has a comparable reconstruction fidelity as the true E-mode displacement field.

The analysis usually uses the density field directly.

measure the power spectrum However, modeling the small-scale inhomogeneities limits to $k < 0.1$ $h/$Mpc. We find the nonlinearities in the displacement field is much more linear than the density field. The correlation of the divergence of the displacement field with the primordial (linear) density field is much better than that of the nonlinear density field.

Displacement decomposition.—In the Lagrangian picture of structure formation, the displacement field $\boldsymbol{s}(\boldsymbol{q}, \tau)$ fully describes the motion of each mass element. The Eulerian position $\boldsymbol{x}$ of a mass element is given by

$$\boldsymbol{x}(\boldsymbol{q}, \tau) = \boldsymbol{q} + \boldsymbol{s}(\boldsymbol{q}, \tau), \qquad (1)$$

where $\boldsymbol{q}$ is the initial Lagrangian position of this mass element. The displacement field $\boldsymbol{s}(\boldsymbol{q})$ can be decomposed into a gradient part and a curl part,

$$\boldsymbol{s}(\boldsymbol{q}) = \boldsymbol{s}_E(\boldsymbol{q}) + \boldsymbol{s}_B(\boldsymbol{q}), \qquad (2)$$

where $\nabla \times \boldsymbol{s}_E = 0$ and $\nabla \cdot \boldsymbol{s}_B = 0$. The gradient part can be completely described by a scalar potential, while the curl part has two independent components.

In the 1D cosmology, the displacement field has only one component though it is a vector field [5]. This allows us to determine the displacement field from the density field, which is a scalar field [6]. However, the motion has three degrees of freedom in 3D instead of one. Since from cosmological observations we only have the density field, we expect to reconstruct the scalar part of the displacement field.

Reconstruction algorithm.—The basic idea is to build a curvilinear coordinate system $\boldsymbol{\xi} \equiv (\xi_1, \xi_2, \xi_3)$, where the mass per volume element is constant. In order to

determine the physical position of each lattice point, we need to specify the Cartesian coordinate $\boldsymbol{x}(\boldsymbol{\xi},\ t)$ of each curvilinear coordinate. Since we attemp to follow the potential flow instead of the vorticity, we define a coordinate transformation that is a pure gradient,

$$x^i = \xi^\mu \delta^i_\mu + \Delta x^i, \tag{3}$$

where

$$\Delta x^i \equiv \frac{\partial \phi}{\partial \xi^\nu} \delta^{i\nu}. \tag{4}$$

Here, Δx^i is the *lattice displacement* and ϕ the *deformation potential* [7, 8]. The new coordinate frame gives the estimated initial Lagrangian coordinates. The difference between these two frames is the estimated nonlinear displacement. Here, Latin indices denote Cartesian coordinate labels x^i, while Greek indices denote the curvilinear coordinates ξ^α.

There are many possible ways to determine the new coordinate frame. One efficient and robust algorithm is the moving grid approach [7, 8]. This approach is originally introduced for the adaptive particle-mesh N-body code [7] and the moving mesh hydrodynamics code [8]. The moving grid based simulation algorithm adopts a curvilinear moving grid which evolves towards a state of constant mass per grid cell. The evolution of the deformation potential is determined by a linear elliptic evolution equation

$$\partial_\mu(\rho\sqrt{g}e^\mu_i\delta^{i\nu}\partial_\nu\dot{\phi}) = \Delta\rho, \tag{5}$$

where e^μ_i is the matrix inverse of the triad $e^i_\mu = \partial x^i/\partial \xi^\mu$, $\sqrt{g} = \det(\partial x^i/\partial \xi^\alpha)$ and $\Delta\rho = \bar{\rho} - \rho\sqrt{g}$. See Ref. [7] for a simple physical intepretation of Eq. (5). The ellpitic equation can be solved using the multigrid algorithm described in Ref. [7].

Since the displacement from the initial Lagrangian coordinate to the final Eulerian coordinate can be large, the elliptic equation must then be solved iteratively. We obtain the change of the deformation potential $\Delta\phi = \dot{\phi}\Delta t$ at each time step and then update the density field in the new Cartesian coordinate frame. The solution is given by

$$\phi = \Delta\phi^{(1)} + \Delta\phi^{(2)} + \Delta\phi^{(3)} + \cdots \tag{6}$$

where $\Delta\phi^{(i)}$ is the result from the ith iteration. We also implement the smoothing and limiting schemes to guarantee the triad e^μ_i is positive definite [7, 8], from which we have the relation $\partial x^a/\partial \xi^a > 0$ (no summation). From this equality, it follows that each Cartesian coordinate increases monotonically as a function of its corresponding curvilinear coordinate. Then, the negative divergence of the estimated displacement gives the reconstructed density field

$$\delta_r(\boldsymbol{\xi}) = -\nabla_{\boldsymbol{\xi}} \cdot \Delta\boldsymbol{x}(\boldsymbol{\xi}) = -\nabla^2_{\boldsymbol{\xi}}\phi(\boldsymbol{\xi}). \tag{7}$$

where $\boldsymbol{\xi}$ is the estimated initial Lagrangian coordinate. In the case that particles follow a irrotational potential flow
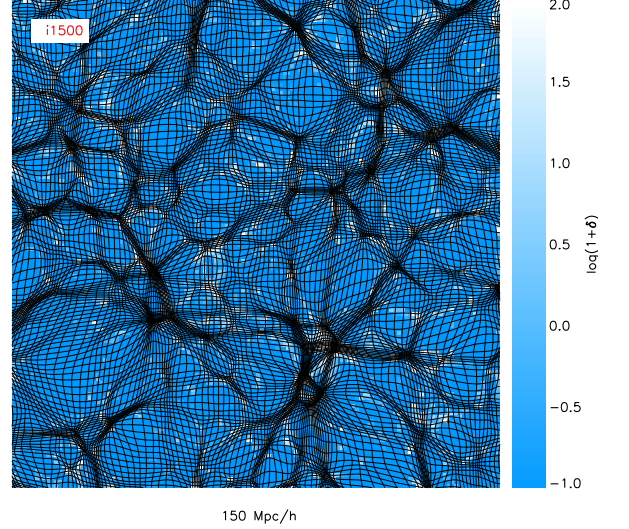

FIG. 1: The nonlinear density field at $z = 0$ and the projected deformed grid from reconstruction. The grid lines show good correlation with the density field.

and no shell crossing happens, the reconstructed displacement is exact up to a global spatial translation. However, shell crossing happens in the nonlinear regime. This reconstruction algorithm gives an effective displacement.

Implementation and results.—To test the performance of the new reconstruction algorithm, we run N-body simulations with the CUBEP^{3}M code [9]. The simulation involves 2048^3 dark matter particles in a box of side length 600 Mpc/h. In the analysis, we use the output at $z = 0$. Mass densities are computed on 512^3 grids. The nonlinear reconstruction code is based on the CALDEFP subroutine from the moving mesh hydrodynamics code [8]. The nonlinear reconstruction code solves the deformation potential iteratively. We test convergence by comparing results from different time steps and find the reconstrution converges after 1500 time steps for the nonlinear density field on 512^3 grids. We also scale the initial density field at $z = 100$ by the linear growth factor to get the linear density field at $z = 0$.

Figure 1 shows a slice of the nonlinear density field. We also overplot the deformed grid on the density field. The grid becomes denser in the higher density region and sparser in the lower density region. The grid lines also show strong correlation with the filementary structures. The difference between the regular grid and the deformed grid is the estimated displacement field, whose divergence gives the reconstructed linear density field. The nonlinear density field $\delta(\boldsymbol{x})$ is given on the Eulerian position $\boldsymbol{x}$, while the reconstructed density field $\delta_r(\boldsymbol{\xi})$ is computed on the estimated Lagrangian position $\boldsymbol{\xi}$. Due to the limiting and smoothing schemes we use, the grid never overlaps itself as in Refs. [7, 8].
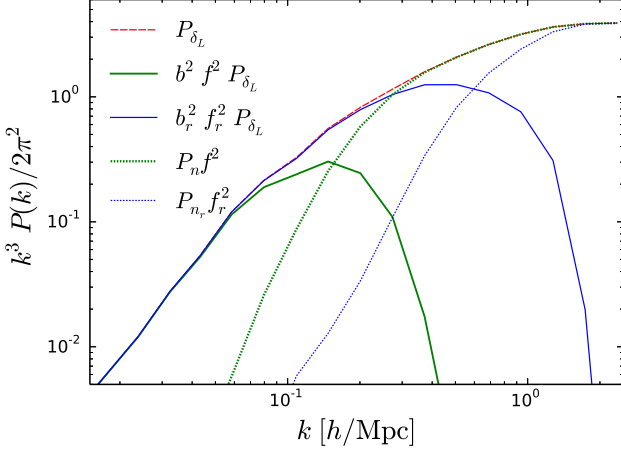
FIG. 2: The linear power spectrum (dashed line), the linear parts of the nonlinear (thick solid line) and reconstructed (thin solid line) power spectra, the noise parts of the nonlinear (thick dotted line) and reconstructed (thin dotted line) power spectra. For visual comparisions, we rescale both the linear and noise parts by $f^2 = P_{\delta_L}/P_\delta$ and $f_r^2 = P_{\delta_L}/P_{\delta_r}$ for the nonlinear and reconstructed fields, respectively. The noise terms dominate over the signals at $k \gtrsim 0.1$ Mpc^{-1} for the nonlinear field and $k \gtrsim 0.6$ Mpc^{-1} for the reconstructed field.

To conveniently quantify the linear information δ_L in the reconstructed density field δ_r, we decompose the reconstructed field δ_r as

$$\delta_r(k) = b_r(k)\delta_L(k) + n_r(k), \qquad (8)$$

where $b_r(k) = P_{\delta_r\delta_L}(k)/P_{\delta_L}(k)$. Here, $b_r\delta_L$ is completely correlated with the linear density field δ_L and n_r uncorrelated with the linear density field δ_L. The power spectrum of the reconstructed field can be written as

$$P_{\delta_r}(k) = b_r^2(k)P_{\delta_L}(k) + P_{n_r}(k), \qquad (9)$$

where b_r^2 is the nonlinear damping factor. For the nonlinear density field, we also have

$$P_\delta(k) = b^2(k)P_{\delta_L}(k) + P_n(k), \qquad (10)$$

where $b(k) = P_{\delta\delta_L}(k)/P_{\delta_L}(k)$. In Fig. 2, we plot the linear components and the noise terms of the nonlinear and reconstructed fields. The noise part dominates over the linear signal at $k \gtrsim 0.6$ Mpc/h, indicating that all BAO peaks can be measured to an unprecented accuracy.

Reconstruction reduces the nonlinear damping $b^2(k)$ as well as the noise term $P_n(k)$. To quantify the overall performance, we can use the cross-correlation coefficient

$$r(k) = \frac{P_{\delta\delta_L}(k)}{\sqrt{P_\delta(k)P_{\delta_L}(k)}} = \frac{1}{\sqrt{1 + \eta(k)}}, \qquad (11)$$

where $\eta = P_n/(b^2 P_{\delta_L})$ quantifies the relative amplitude of n with respect to $b\delta_L$. In Fig. 3, we plot the cross-correlation coefficients. The correlation of the reconstructed field δ_r with the linear density field δ_L is almost
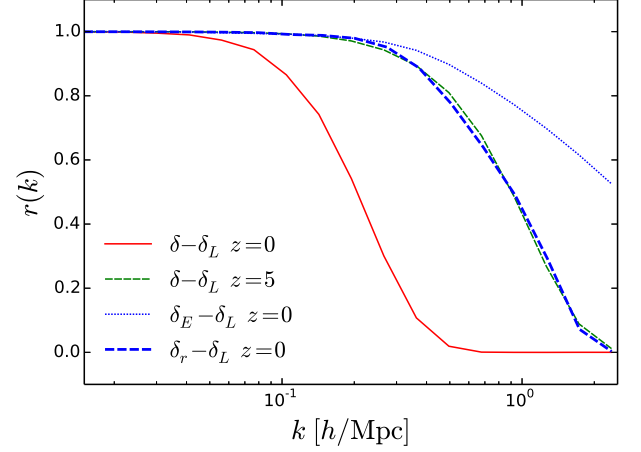

FIG. 3: The $\delta - \delta_L$ correlation coefficients at $z = 0$ (solid line) and $z = 5$ (thin-dashed line), the $\delta_E - \delta_L$ correlation coefficient (dotted line), as well as the $\delta_r - \delta_L$ correlation coefficient (thick-dashed line).

the same as that of the nonlinear density field δ at $z = 5$, which is better than the 1D case, where the correlation of δ_r with δ_L is only comparable to that of δ at $z = 3$ [6]. This is also as expected since the nonlinear evolution in 1D is more significant than the 3D case [5]. We also show the cross-correlation coefficient of δ_E with δ_L, where $\delta_E(\boldsymbol{q}) = -\nabla \cdot \boldsymbol{s}_E(\boldsymbol{q})$ is the negative divergence of the real displacement from simulation. It is still hard to recover linear modes at $k \gtrsim 1h/$Mpc, since some information has been irreversibly lost in nonlinear evolution.

The density fluctuation probability distribution function (PDF) quantifies the Gaussianity of the density field. Figure 4 shows the PDFs of the density fields. Since the PDFs depend on the grid scale, we apply the Wiener filter

$$W(k) = \frac{P_{\delta_L}(k)}{P_{\delta_L}(k) + P_{n_r}(k)/b_r^2(k)} \qquad (12)$$

to both the reconstructed and linear fields to get the converged results. The reconstructed density field is well correlated with the linear density field and also much more Gaussian than the original nonlinear density field. The new reconstruction method are expected to reduce the correlation in the covariance matrix and increase the information content of the power spectrum [10–12]. Notice that the values of the reconstructed density field δ_r are always smaller than 3. The compression limiter constrains $\partial x^a/\partial \xi^a \geq 0.1$ [7, 8]. The reconstructed density field is given by the negative divergence of the estimated nonlinear displacement field $\delta_r = -\nabla \cdot \Delta \boldsymbol{x} = 3 - \nabla \cdot \boldsymbol{x}$, where $\nabla \cdot \boldsymbol{x} = \partial x^1/\partial \xi^1 + \partial x^2/\partial \xi^2 + \partial x^3/\partial \xi^3$. We find the maximum value is 2.7 for the reconstructed density field. This has confirmed that we have a continuous sequence of nondegenerate triads in the reconstruction. In the 1D case, the maximum value is 1 since we only have one spatial dimension in the 1D cosmology [6].
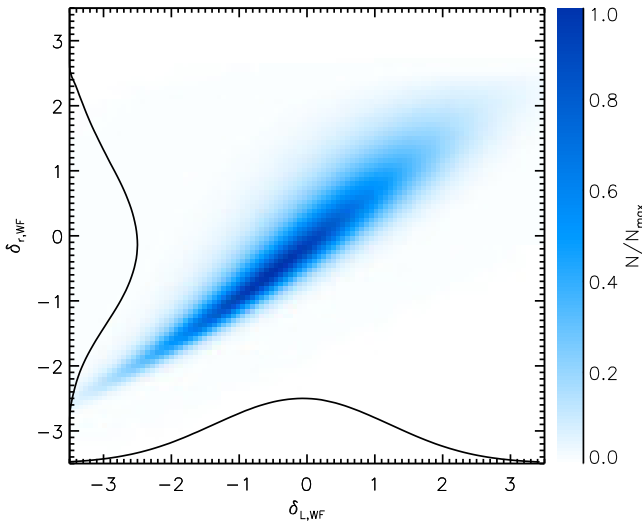
FIG. 4: The joint probability distribution function of the reconstructed field δ_r and linear density field δ_L. We also plot the probability distrbution functions of δ_r and δ_L. Both fields have been Wiener filtered to get converged results. The value of the reconstructed density field is always smaller than 3.

Discussions.—The new reconstruction method reduces the nonlinearities significantly and successfully recovers a lot of linear modes at $k < 0.6$ h/Mpc, which is about all the linear BAO information. This has significant implications for measuring BAO in the current and future surveys, especially for volume-limited galaxy samples. To apply the new reconstruction method to observations, we need to consider reconstruction from galaxy density fields with redshift space distortions. The modelling of the reconstructed density field will also be simplified since less nonlinear effects are involved in the current method. We intend to investigate these in subsequent works.

The new method is also useful for improving the measurement of redshift space distortions. The nonlinear displacement is much more linear than the nonlinear density field. This also simplifies the modelling of RSD, which is usually limited by nonlinearities [13]. The current method to reconstruct velocity field from the observed density fieldis derived from the linearized continuity equation. The nonlinear density field is usually smoothed on the linear scale (~ 10 Mpc/h) to make the linear approximation valid. We can also reconstruct the velocity field from the estimated displacement field. This requires a detailed study of the correlation between the displacement field and the velocity field, which will be presented in future.

Neutrinos are expect to suppress the growth of structure on scales below the neutrino thermal free-streaming scale [14, 15]. It is interesting to study the effect of neutrinos on the Lagrangian space clustering. The new method is also crucial for measuring the dark matter-neutrino cross correlation dipole [16, 17].

ELUCID [18]? The reconstructed nonlinear displacement can be further improved ...?

[1] U.-L. Pen, R. Sheth, J. Harnois-Deraps, X. Chen, and Z. Li, ArXiv e-prints (2012), 1202.5804.

[2] H.-M. Zhu, U.-L. Pen, Y. Yu, X. Er, and X. Chen, Phys. Rev. D **93**, 103504 (2016), 1511.04680.

[3] Y. Li, W. Hu, and M. Takada, Phys. Rev. D **90**, 103530 (2014), 1408.1081.

[4] D. J. Eisenstein, H.-J. Seo, E. Sirko, and D. N. Spergel, ApJ **664**, 675 (2007), astro-ph/0604362.

[5] M. McQuinn and M. White, J. Cosmology Astropart. Phys. **1**, 043 (2016), 1502.07389.

[6] H.-M. Zhu, U.-L. Pen, and X. Chen, ArXiv e-prints (2016), 1609.07041.

[7] U.-L. Pen, ApJS **100**, 269 (1995).

[8] U.-L. Pen, ApJS **115**, 19 (1998), astro-ph/9704258.

[9] J. Harnois-Déraps, U.-L. Pen, I. T. Iliev, H. Merz, J. D. Emberson, and V. Desjacques, MNRAS **436**, 540 (2013), 1208.5098.

[10] A. Meiksin and M. White, MNRAS **308**, 1179 (1999), astro-ph/9812129.

[11] R. Scoccimarro, M. Zaldarriaga, and L. Hui, ApJ **527**, 1 (1999), astro-ph/9901099.

[12] C. D. Rimes and A. J. S. Hamilton, MNRAS **360**, L82 (2005), astro-ph/0502081.

[13] P. Zhang, J. Pan, and Y. Zheng, Phys. Rev. D **87**, 063526 (2013), 1207.2722.

[14] J. R. Bond, G. Efstathiou, and J. Silk, Physical Review Letters **45**, 1980 (1980).

[15] W. Hu, D. J. Eisenstein, and M. Tegmark, Physical Review Letters **80**, 5255 (1998), arXiv:astro-ph/9712057.

[16] H.-M. Zhu, U.-L. Pen, X. Chen, D. Inman, and Y. Yu, Physical Review Letters **113**, 131301 (2014), 1311.3422.

[17] H.-M. Zhu, U.-L. Pen, X. Chen, and D. Inman, Physical Review Letters **116**, 141301 (2016).

[18] H. Wang, H. J. Mo, X. Yang, Y. P. Jing, and W. P. Lin, ApJ **794**, 94 (2014), 1407.3451.